Journal of Radiological Protection

Official journal of the Society for Radiological Protection

PAPER

Monte Carlo modelling of cyclotron and radioisotope center (CYRIC) at Tohoku University: a radiation protection study

To cite this article: Hiroshi Watabe *et al* 2024 *J. Radiol. Prot.* **44** 021521

IOP Publishing J. Radiol. Prot. **44** (2024) 021521 https://doi.org/10.1088/1361-6498/ad5450

Journal of Radiological Protection

CrossMark

RECEIVED
8 February 2024

REVISED
18 May 2024

ACCEPTED FOR PUBLICATION
5 June 2024

PUBLISHED
13 June 2024

PAPER

Monte Carlo modelling of cyclotron and radioisotope center (CYRIC) at Tohoku University: a radiation protection study

Hiroshi Watabe[1], Peter K N Yu[2], Gary Tse[3], Dragana Krstic[4], Dragoslav Nikezic[4], M Rafiqul Islam[1,5], Zhanbing Wei[6], Yuezhou Wei[1,6] and Mehrdad Shahmohammadi Beni[1,2,3,*]

[1] Division of Radiation Protection and Safety Control, Cyclotron and Radioisotope Center, Tohoku University, 6-3 Aoba, Aramaki, Aoba, Sendai, 980-8578 Miyagi, Japan
[2] Department of Physics, City University of Hong Kong, Tat Chee Avenue, Kowloon Tong, Hong Kong Special Administrative Region of China, People's Republic of China
[3] School of Nursing and Health Studies, Hong Kong Metropolitan University, Homantin, Kowloon, Hong Kong Special Administrative Region of China, People's Republic of China
[4] Faculty of Science, University of Kragujevac, R. Domanovica 12, 34000 Kragujevac, Serbia
[5] Institute of Nuclear Medical Physics, AERE, Bangladesh Atomic Energy Commission, 1349, Dhaka, Bangladesh
[6] School of Nuclear Science and Technology, University of South China, 28 Changsheng, West Road, Hengyang, 421001, Hunan, People's Republic of China
[*] Author to whom any correspondence should be addressed.

E-mail: ben.sh@tohoku.ac.jp, watabe@cyric.tohoku.ac.jp, appknyu@cityu.edu.hk, gatse@hkmu.edu.hk, dragana@kg.ac.rs, nikezic@kg.ac.rs, mripbaec@baec.gov.bd, 20232005210314@stu.usc.edu.cn and yzwei@usc.edu.cn

Keywords: Monte Carlo method, radiation protection, ionizing radiation, cyclotron

Abstract

Protection against ionizing radiations is important in laboratories with radioactive materials and high energy cyclotron beams. The Cyclotron and Radioisotope Center (CYRIC) located in Tohoku University in Miyagi prefecture, Japan and is a well-known nuclear science laboratory with cyclotron beams and substantial number of high activity radioactive materials. Considering this, it is important to perform complete radiation transport computations to ensure the safety of non-occupational and occupational workers. In the present work, we have developed a complete 3-dimensional model of the main cyclotron building and radiation labs using Monte Carlo method. We have found that the dispersed photons and neutrons inside and in the surrounding of the CYRIC building pose no significant risk to occupational and non-occupational workers. The present work and the developed models would be useful in the field of radiation protection.

1. Introduction

Protection against ionizing radiation is an important step toward limiting the absorbed dose in occupational and non-occupational workers (the term occupational and non-occupational workers refers to those occupationally exposed personnels, and the member of the public, respectively) [1–7], which aligns with the general objective to reducing the detrimental effect on living organisms [8–10]. In nuclear research centers, radioactive materials and/or accelerator beams will lead to the emission of primary and secondary ionizing radiations. Considering this, the effectiveness of the shielding materials embedded in buildings containing the radioactive materials and/or accelerator beams would be very important to general public and those occupational workers [11, 12].

The Cyclotron and Radioisotope Center (CYRIC) located in Tohoku University in Miyagi prefecture, Japan [13] is a well-known nuclear science laboratory with cyclotron beams and substantial number of high activity radioactive materials. The photons and neutrons emitted from radioactive sources and generated from the cyclotron are highly penetrative [14, 15]. Considering this, it would be pertinent to perform a complete radiation transport and protection study to ensure the safety of non-occupational and occupational workers. Previously, researchers studied the absorbed dose rate in air due to gamma radiation from building materials by modeling various dwelling structures [16]. Furthermore, a detailed Monte Carlo N-Particle (MCNP) model of the ITER Tokamak Complex was created [17] for radiation transport and protection investigations. Similarly, Sharma *et al* [18] utilized the MCNP package to model the neutron generator and its shielding at Missouri University of Science and Technology.

In the present work we have developed a complete 3-dimensional model of the main cyclotron building as well as restricted radiation area and its neighboring offices. An open-source computer program named CyricSim (stands for CYRIC Simulator) was developed to generate the 3-dimensional model. The CyricSim model enables users to choose the source location in two different modes, namely, (1) radioisotope and (2) cyclotron modes. In addition, neutron and photon tallies would be automatically generated in the prespecified locations. The present program was coupled with the well-established particle and heavy ion transport code system (PHITS) (https://phits.jaea.go.jp/) Monte Carlo (MC) package, which then was used to study the radiation transport and interaction in the modelled domain. The obtained results, methodology and the developed tools would be useful for radiation protection studies in CYRIC laboratories and also other nuclear radiation labs worldwide.

2. Materials and methods

In present work, an open-source computer program named CyricSim (stands for CYRIC Simulator) has been developed. The present program was written in FORTRAN90 programming language and coupled with the PHITS MC package. The users have the ability to control the geometrical, material, type of ionizing radiation and MC parameters through a configuration file. The program will read the user inputs from the configuration file and generate a 3-dimensional model accordingly. The details regarding the developed program and computational scheme were provided in the following subsections.

2.1. CyricSim program

The CyricSim program was written in FORTRAN90 programming language and has ~1800 lines of code. There are total of three subroutines, namely, (1) readconfig (read the user input configuration file), (2) cymap (generates a terminal-based map) and (3) cygen (generates the actual 3-dimensional model and PHITS script). The configuration file takes total of 18 user inputs that are; (1) first floor wall height, (2) second floor wall height, (3) wall thickness, (4) floor thickness, (5) wall material file, (6) density of the wall material, (7) cyclotron mode on/off option, (8) cyclotron beamline room, (9) radioisotope mode on/off option, (10) radioisotope definition file, (11) option for time evolution (dtime) value for specific radioisotope, (12) radioisotope room location, (13) particle tally type, (14) tally positions file, (15) number of histories per batch (maxcas), (16) number of batches (maxbch), (17) number of Message Passing Interface Central Processing Unit cores and (18) output filename.

In present work, we have set the first floor wall height to 600 cm, second floor wall height to 300 cm, wall thickness to 31.5 cm and floor thickness to 30 cm. Similar to our previous work [12], the wall and floor material was assumed to be composed of ordinary concrete with density of 2.40 g cm^{-3}. Furthermore, the ambient material was assumed to be dry air with density of 0.00 129 g cm^{-3}. The material compositions of the concrete and dry air that were used in the present model were summarized in table 1.

2.2. Radioisotope and cyclotron modes

The two main operational mode for CyricSim model are, (1) radioisotope and (2) cyclotron modes. In case of the radioisotope mode, a point source with RI function of PHITS MC package will be used; this is similar to the point source definition employed in our previous works [19, 20]. The RI function in the source definition will generate an isotropic point source (spherical in geometry) with a radius of 10^{-10} cm; this emits radiation in all directions in spatial 3-dimensional coordinate system. This source has been defined using the s-type 9 function provided by the PHITS MC package. In addition, the energy distribution of radionuclide has been defined using e-type 28 PHITS function that automatically and accurately determines each radioisotope energy spectrum. The point source in the radioisotope mode can be placed in any of the modelled rooms. The source will be automatically placed at the center of the room and 5 cm above the floor . The radioactive source parameters such as radionuclides, activity and time evolution can be set by the user.

In the case of the cyclotron mode, a disk source with radius of 0.5 cm emitting protons will be used to irradiate a copper (Cu) block; this is used experimentally to generate a neutron beam from incident proton beam accelerated by the cyclotron. The parameters of the cyclotron room that contains the beamline can be chosen by the users; these were shown in figure 1. For simplicity, we have assumed perpendicular irradiation of the copper block at its center so that the generated secondary neutrons and photons will be emitted in an isotropic fashion. In this case, default physics card for transport and interaction of primary protons and secondary photons and neutrons were used. In this case, the proton, neutron and photon cutoff energies were 10^{-3}, 10^{-11} and 10^{-3} MeV, respectively. Furthermore, the JENDL photo-nuclear data library provided by the PHITS package was used in this study. We refer the interested reader to PHITS documentation for

Table 1. Material composition of the ordinary concrete and dry air used in the present model. (All composition fractions are in weight percent).

Material	^{1}H	^{12}C	^{14}N	^{16}O	^{23}Na	^{24}Mg	^{27}Al	^{28}Si	^{39}K	^{40}Ca	^{56}Fe	Other
Concrete	0.02	0.002	—	0.57	0.015	0.0013	0.02	0.28	0.01	0.04	0.006	0.0357
Dry Air	—	—	0.77	0.23	—	—	—	—	—	—	—	—

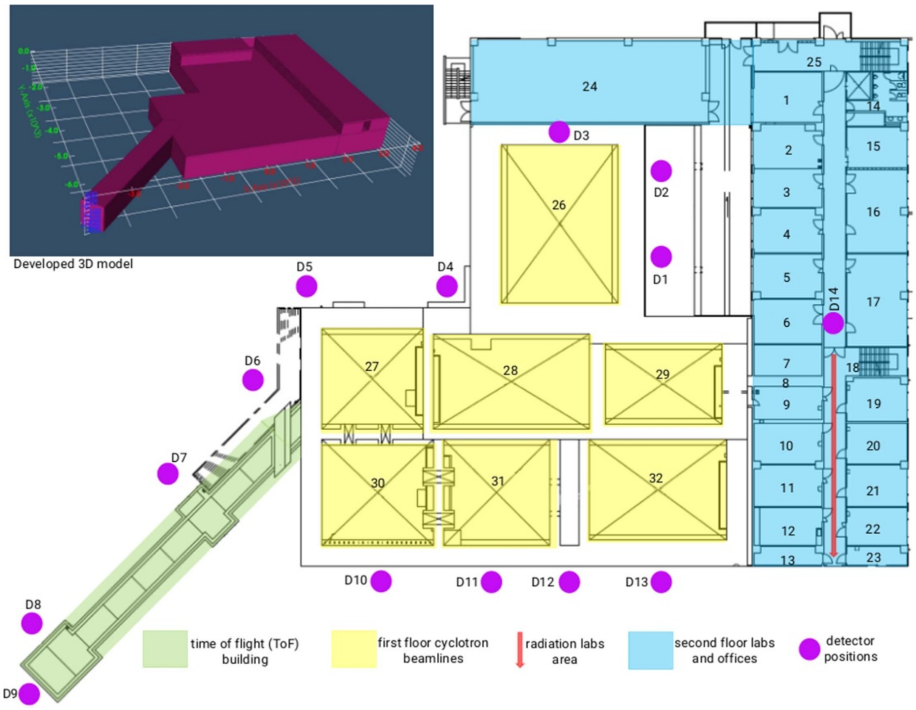

Figure 1. The map of the CYRIC cyclotron building including restricted radiation area and its neighboring offices (rooms 1 to 25). The cyclotron beamline rooms (rooms 26 to 32) and point detector locations are also shown.

more information at: https://phits.jaea.go.jp/manual/manualE-phits.pdf The incident energy of the proton beam emitted from the cyclotron was set to 80 MeV, which is the maximum operational energy used in the cyclotron at CYRIC.

2.3. Photon and neutron tallies

The modelled point detector was placed around the modelled domain shown in figure 1, and the energy distributions of the photons and neutrons were scored. The minimum and maximum energy bins were set to 1×10^{-10} and 100 MeV, respectively. Total number of bins was set to 100, which determines the particle flux per source particle versus energy. Total of 15 point detectors with radius of 10 cm were placed at predefined locations in the modelled domain. The choice of detector radius was mainly based on the size of Snyder head phantom [21] and average height of the human head [22]. These average values were rounded up and used as the radius of the detector. It also needs to be noted that the detector radius can be changed by the users to match their desired size for specific cases. The first point detector was placed in close proximity of the radioactive source (for the radioisotope mode) or cyclotron beam (for the cyclotron mode); this enabled the determination of a baseline reading for the energy spectrum for photons and neutrons. This baseline spectrum was then used to normalize the point detector results at different locations. The results shown in figure 5 were normalized by determining the total flux fraction. This involved dividing the total flux for all energy bins at specific detector locations by the total flux for all energy bins measured in close proximity to the source (CPS). The 2-dimensional map of the modelled domain with point detector locations is shown in figure 1. Considering the radioisotope case, where the source activity is defined in the PHITS package, and the unit of the obtained flux values is cm^{-2}/source. This unit takes into account the source activity (number of emitted particles per second), which in this case was set to 60 MBq. For other results, the flux values were normalized to the number of incident particles, so the results are presented in cm^{-2}/incident particle.

2.4. Benchmarking with MCNP 6.3

In order to benchmark and validate our developed model, we have modified the generated code from CyricSim to run on MCNP package. Currently, the time-of-flight building is not operational. Therefore, for simplicity, we omitted it in our benchmarking with MCNP. This was mainly to concentrate on the radiation areas that accommodate researchers and radiation workers in the main buildings. The MCNP version 6.3 was used to perform the benchmarking. For this benchmarking, a ^{137}Cs point source with a photon energy of 0.661 MeV was placed in room 10 (denoted as R10) and 22 (denoted as R22) (see figure 1). The particle flux (in this case photons) in CPS and 14 point detectors were determined from our model and those from MCNP version 6.3 package.

2.5. Computational scheme

In order to present the capability of the present model and employed methodology, we have chosen a number of examples from radioisotope and cyclotron modes. In total four cases were considered, two cases for each operational mode. For the radioisotope mode cases, a ^{137}Cs radioactive source with activity of 60 MBq has been considered. For case 1, the source was placed in room 10 which is the restricted radiation area in CYRIC and located on the second floor. For case 2, the same source was placed in room 22 which is also the restricted radiation area in CYRIC and located on the second floor. For the cyclotron mode cases, a copper block will be irradiated perpendicularly with 80 MeV incident proton beam in cyclotron rooms as shown in figure 1. For cases 1 and 2, the irradiations were assumed to take place in cyclotron room 28 and 30, respectively. These rooms are located on the ground floor and host the cyclotron beamline in CYRIC. For the radioisotope case involving a ^{137}Cs source, an isotropic point source was modeled. For the cyclotron case, a pencil-like disk source with a diameter of 1 cm emitting radiation toward a copper block was used. In this study, no specific collimators were considered for either case.

For both radioisotope and cyclotron cases, photon and neutron tallies discussed in the previous section will be used to determine the energy distribution of the generated neutrons and photons at different preselected locations. In addition to the energy distribution, the total flux fraction that was summed over the considered energy grid from 1×10^{-10} and 100 MeV has been determined; this will be particularly useful for evaluation of flux reduction when compared to the particle flux in the CPS. At last, the total flux fraction was calculated by summing all the flux values in all energy bins for all 14 detector positions (i.e. D1 to D14) and divided by the sum of flux values for the detector that was placed at the CPS. In this study, the number of emitted particles, also known as the number of histories, was set to 10^6 incident particles for all cases. The relative errors obtained from the tallies are represented as error bars in the results.

3. Results and discussion

The benchmarking results from the comparison of particle flux in total of 15 different detector positions between our model and those from MCNP were determined and shown in figure 2. From the comparison shown in figure 2, the results from our model and those from MCNP6.3 are in a good agreement for CPS and most other 14 different detector positions. The differences between our model and those from MCNP6.3 appear to fall within the error bars for detector positions D1, D2, and D3, which are located on the first floor. Notably, the incident particles emitted from the source in the R10 and R22 cases are significantly attenuated by the time they reach detector positions D1, D2, and D3. This attenuation occurs due to the multiple concrete slabs between the second and first floors, resulting in a low interaction efficiency at these positions. Considering this, it can be concluded that our model has the ability to accurately estimate the particle flux in the modelled CYRIC domain.

For the radioisotope mode with the presence of a 60 MBq ^{137}Cs radioactive source, the energy distributions of photons in CPS and 14 different detector positions have been determined. The results of the energy distribution for both case 1 and 2 are shown in figure 3. The flux at CPS was found to be highest in both cases, mainly due to the proximity of the point detector to the radioactive source.

It needs to be noted that the flux values tend to reduce in detectors that are distant from the radioactive source, mainly due to the increased distance and attenuation of incident photons by concrete walls, floors and ceilings. Considering the position of the radioactive source which is placed on the second floor of the modelled building, the lowest flux values were obtained in detectors D1 to D3 which are located inside the cyclotron building on the first floor and concealed by the concrete ceiling. For other detectors (except detector 14), the flux values were found to be not very different, given that they are placed outside of the modelled building. For detector 14, the flux values tend to be higher for most photon energies in case 1, as it is located on the second floor and closest to room 10. It is important to note that, the flux values and the energy of photons were significantly reduced (several orders of magnitude) in all 14 detectors; this shows that the concrete shielding has the ability to effectively attenuate the ionizing radiation emitted by the ^{137}Cs

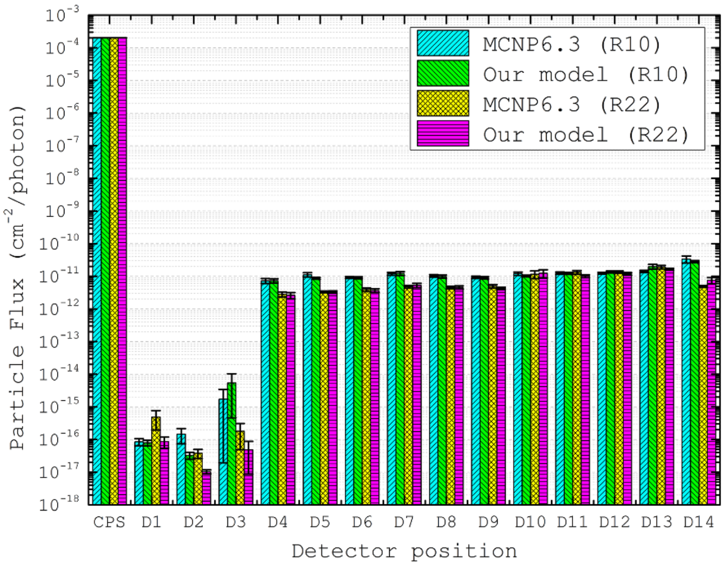

Figure 2. The comparison of particle flux in close proximity to the source (CPS) and 14 deterctor positions for source location in room 10 (R10) and room 22 (R22) from our model and MCNP6.3 package.

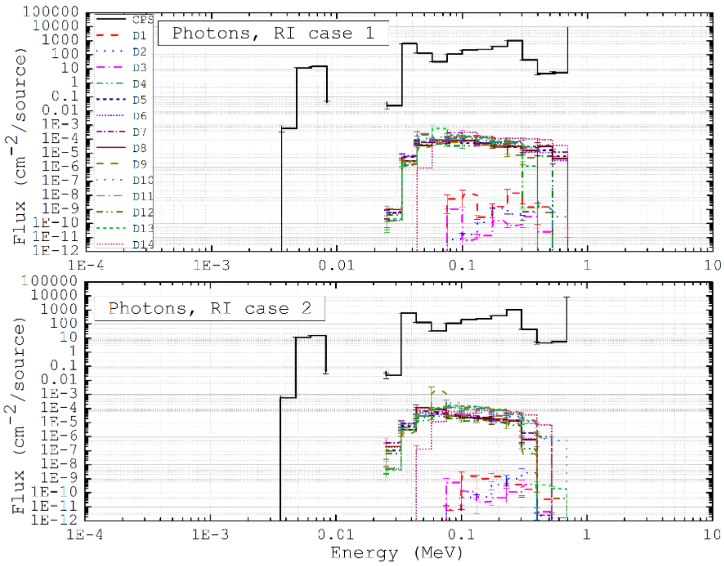

Figure 3. The energy distributions of photons obtained from different point detectors as a result of 60 MBq ^{137}Cs radioactive source placed in room 10 and 22 for case 1 and 2, respectively.

radioactive source. Considering the present results, it can be concluded that the amount of dispersed ionizing radiation from the radiation laboratory in CYRIC with radioisotopes such as the ^{137}Cs radioactive source would be negligible outside the restricted radiation area. As outlined in the inverse square law, the intensity of a quantity (such as flux) is inversely proportional to the square of the distance from point like source. Hence, the distance between the detector and the source is a crucial factor in the analysis.

For the cyclotron mode with the 80 MeV proton irradiation of a copper block, the energy distributions of the photons and neutrons have been determined. The obtained photon and neutron energy distributions for case 1 and 2 are shown in figures 4(a) and (b), respectively. It needs to be noted that the flux of these neutral secondary emitted particles are highly important at distances further away from their points of creation, given that photons and neutrons generated as a result of proton irradiations usually have large mean free paths. The flux of photons and neutrons in close proximity of the source (CPS) and 14 different detector positions (see figure 1) have been determined.

The highest and lowest flux values were scored at CPS and D14 positions, respectively. The D14 detector is located on the second floor of the modelled CYRIC building and therefore the generated secondary photons and neutrons would be significantly attenuated before reaching the detector located at D14 position.

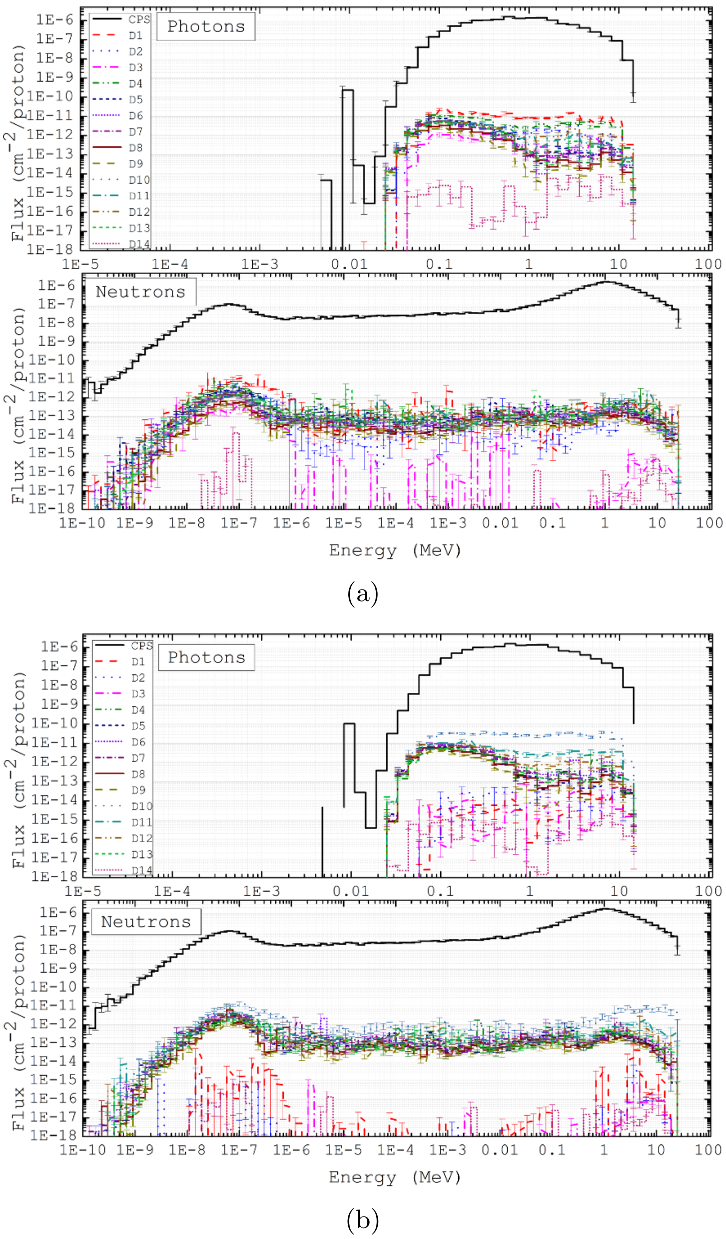

Figure 4. Energy distributions of the secondary photons and neutrons emitted from cyclotron irradiation of copper block for (a) case 1 and (b) case 2.

For case 1, the flux at D1 and D4 detector positions were found to be higher when compared to other detector positions; this is main due to the close proximity of D1 and D4 detector position to the irradiation room number 28 (see figure 1). However, in case 2 at which the irradiation was assumed to occur in room number 30 (see figure 1), the highest flux values were detected at D10 detector position which is closest to the irradiation room.

It is worth noting that the high-energy part of the energy distribution results decreases for both photons and neutrons. This decrease is a result of the subsequent scattering of these particles with concrete walls, floors, and ceilings, which in turn reduces the energy of the scattered particles. The results for case 1 and 2 show that the flux of particles away from the irradiation rooms decrease significantly (by several orders of magnitude). In order to better present the reduction in the particle flux for all the cases, the total flux fraction has been determined and shown in figure 5. The total flux fraction was determined for 5 different detector locations, namely, (1) D1, (2) D5, (3) D9, (4) D12 and (5) D14 (see figure 1).

All the obtained total flux fraction values were found to be lower than 0.01% and the highest total flux fraction was obtained at D1 detector position for case 1 cyclotron irradiation; this was due to the short distance between the D1 detector position and case 1 cyclotron irradiation. Considering the D5 position, the total flux fraction for both case 1 and 2 of the cyclotron irradiations are close to one another mainly due to

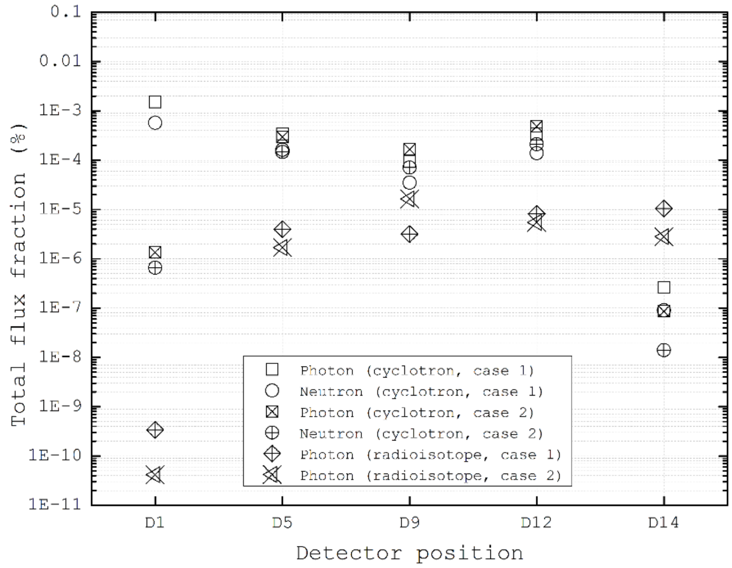

Figure 5. The total flux fraction determined for all cases at D1, D5, D9, D12 and D14 detector positions (see figure 1).

the similar distance from point of irradiation and the detector position (see figure 1). Similar trend can be observed at D9 and D12 detector positions at which the total flux fraction for case 1 and 2 of the cyclotron irradiation are not significantly different. The lowest total flux fraction for cyclotron irradiation cases was found to be in D14 detector position, which is located on the second floor of the modelled CYRIC building and is the furthest detector from the irradiation points.

For the total flux fraction for the case 1 radioisotope irradiation, the highest value was detected at the D14 detector position. Interestingly, the total flux fraction values were found to be highest at D9 detector position for case 2 radioisotope irradiation. The lowest total flux fraction was obtained in D1 detector position, given that D1 detector is placed inside the cyclotron building and the photons would be significantly attenuated before reaching the D1 detector. It also needs to be noted that the total flux fraction significantly decreases (several orders of magnitude) for all detector positions as shown in figure 5. Therefore, for both cyclotron and radioisotope irradiations, the dispersed ionizing radiation inside and in the surrounding of the CYRIC building pose no significant risk to occupational and non-occupational workers. In our laboratory, we conduct cyclic measurements of activated concrete materials by sampling them. This process is crucial yet challenging, as it requires maintaining the integrity of the concrete while collecting samples to assess photon and neutron-induced activity. The current model does not account for the impact of activated concrete materials, as this falls outside the scope of our study. In future research, we plan to explore the use of nanomaterials or alloy materials to reduce the thickness of concrete while maintaining or enhancing its shielding effectiveness against ionizing radiation.

4. Conclusions

This study presents a detailed 3-dimensional model of the CYRIC radiation laboratory at Tohoku University, Miyagi Prefecture, Japan, considering both radioisotope sources and cyclotron irradiation modes. We analyzed the energy distributions of photons and neutrons at 14 different detector positions. Our findings indicate that existing shielding measures effectively minimize the received dose of ionizing radiation, as evidenced by the significant reduction in flux and energy of photons and neutrons with increasing distance from the radiation source. Nonetheless, any modifications to the thickness, material, or density of the concrete shielding could impact its effectiveness in attenuating radiation. Increasing the thickness or utilizing materials with superior attenuation properties could further decrease the radiation dose for individuals within and around the facility. In future research, we plan to integrate human phantom models with our program to assess organ-specific doses for various shielding materials and thicknesses.

Data availability statement

The data that support the findings of this study are openly available at the following URL/DOI: https://figshare.com/articles/software/Monte_Carlo_modelling_of_Cyclotron_and_Radioisotope_Center_CYRIC_at_Tohoku_University_A_Radiation_Protection_Study/24486442.

Acknowledgments

The present work was supported by the JSPS KAKENHI Grant Numbers 21F21103, JPJSBP120218804, 23H03774 and 23K07087, the research Grants 9229151 and 9220124 from City University of Hong Kong and the ministry of education and ministry of science, technological development and innovation, Republic of Serbia, Grants: No. 451-03-47/2023-01/ 200122.

Conflict of interest

The authors declare that they have no conflict of interest.

ORCID iD

Mehrdad Shahmohammadi Beni https://orcid.org/0009-0006-4736-0670

References

[1] Fournier L, Clěro E, Samson E, Caër-Lorho S, Laurier D and Leuraud K 2018 Impact of considering non-occupational radiation exposure on the association between occupational dose and solid cancer among French nuclear workers *Occup. Environ. Med.* **75** 199–204
[2] Wakeford R 2009 Radiation in the workplace-a review of studies of the risks of occupational exposure to ionising radiation *J. Radiol. Prot.* **29** A61–A79
[3] Karipidis K K, Benke G, Sim M R, Kauppinen T and Giles G 2007 Occupational exposure to ionizing and non-ionizing radiation and risk of glioma *Occup. Med.* **57** 518–24
[4] Karipidis K K *et al* 2007 Occupational exposure to ionizing and non-ionizing radiation and risk of non-Hodgkin lymphoma *Int. Arch. Occup. Environ. Health* **80** 663–70
[5] Maghsoudi B, Mortazavi S M, Khademi S and Vatankhah P 2017 Evaluation of radiation exposure pattern and radiation absorbed dose resulting from occupational exposure of anesthesiologists to ionizing radiation *J. Biomed. Phys. Eng.* **7** 271–8
[6] Lee W J, Ko S, Bang Y J, Choe S-A, Choi Y and Preston D L 2021 Occupational radiation exposure and cancer incidence in a cohort of diagnostic medical radiation workers in South Korea *Occup. Environ. Med.* **78** 876–83
[7] Chartier H, Fassier P, Leuraud K, Jacob S, Baudin C, Laurier D and Bernier M-O 2020 Occupational low-dose irradiation and cancer risk among medical radiation workers *Occup. Med.* **70** 476–84
[8] Desouky O, Ding N and Zhou G 2015 Targeted and non-targeted effects of ionizing radiation *J. Radiat. Res. Appl. Sci.* **8** 247–54
[9] Cerutti P A 1974 Effects of ionizing radiation on mammalian cells *Sci. Nat.* **61** 51–59
[10] Ryan J L 2012 Ionizing radiation: the good, the bad and the ugly *J. Invest. Dermatol.* **132** 985–93
[11] Shahmohammadi Beni M, Watabe H, Krstic D, Nikezic D and Yu K N 2021 MCHP (Monte Carlo+ Human Phantom): platform to facilitate teaching nuclear radiation physics *PLoS One* **16** e0257638
[12] Shahmohammadi Beni M, Ng C Y, Krstic D, Nikezic D and Yu K N 2017 Conversion coefficients for determination of dispersed photon dose during radiotherapy: NRUrad input code for MCNP *PLoS One* **12** e0174836
[13] Wakui T, Itoh M, Shimada K, Yoshida H P, Shinozuka T and Sakemi Y 2014 Restoration of accelerator facilities damaged by great east Japan earthquake at cyclotron and radioisotope center, Tohoku university *Tohoku J. Exp. Med.* **233** 221–31
[14] Windsor C G and Morgan J G 2017 Neutron and gamma flux distributions and their implications for radiation damage in the shielded superconducting core of a fusion power plant *Nucl. Fusion* **57** 116032
[15] Amirabadi E A, Salimi M, Ghal-Eh N, Etaati G R and Asadi H 2013 Study of neutron and gamma radiation protective shield *Int. J. Innov. Appl. Stud.* **3** 1079–85
[16] de Jong P and van Dijk W 2008 Modeling gamma radiation dose in dwellings due to building materials *Health Phys.* **94** 33–42
[17] López-Revelles A J, Catalán J P, Kolšek A, Juárez R, García R, García M and Sanz J 2018 MCNP model of the ITER Tokamak Complex *Fusion Eng. Des* **136** 859–63
[18] Sharma M K, Alajo A B and Liu X 2014 MCNP modeling of a neutron generator and its shielding at Missouri university of science and technology *Nucl. Instrum. Methods Phys. Res.* A **767** 126–34
[19] Yu K N *et al* 2023 DynamicMC: an open-source GUI program coupled with MCNP for modeling relative dynamic movement of radioactive source and ORNL phantom in a 3-dimensional radiation field *Health Phys.* **124** 301–9
[20] Watabe H *et al* 2024 Development of dynamicMC for PHITS Monte Carlo package *Radiat. Prot. Dosim.* **200** 130–42
[21] Goorley J T, Kiger Iii W S and Zamenhof R G 2002 Reference dosimetry calculations for neutron capture therapy with comparison of analytical and voxel models *Med. Phys.* **29** 145–56
[22] Makris N, Angelone L, Tulloch S, Sorg S, Kaiser J, Kennedy D and Bonmassar G 2008 MRI-based anatomical model of the human head for specific absorption rate mapping *Med. Biol. Eng. Comput.* **46** 1239–51